Evaporation of Boron from aluminoborosilicate melt

Flemetakis, S., Renggli, C., Pangritz, P., Berndt, J., Klemme, S.

Institut für Mineralogie, Westfälische-Wilhelms-Universität Münster, Corrensstrasse 24, 48149 Münster, Germany

Abstract

We present the results of B_2O_3 evaporation experiments from Ca- and Mg-bearing aluminoborosilicate melts. Our experiments were conducted at 1250 and 1350 °C for different run times (60-1020h), and at oxygen fugacities (logfO_2) relative to the fayalite-magnetite-quartz buffer (FMQ) of FMQ-6 to FMQ+1.5, and in air. Our results show that with increasing fO_2 evaporation of B from the melt increases by an order of magnitude compared to reducing conditions. Using Gibbs free energy minimization calculations, we suggest two possible evaporation reactions for B_2O_3 which constrain its speciation in the gas phase to be either 3+ or 4+ ($B_2O_{3(g)}$, and $BO_{2(g)}$). The measured B_2O_3 contents of the final glasses were used to calculate evaporation rate constants (k_i) for B_2O_3 at oxidizing (air, $k_i = 2.2x10^{-5}$ cm/min at 1350 °C) and reducing conditions (FMQ-4, $k_i = 3.5x10^{-6}$ cm/min at 1350 °C). The absence of diffusion profiles in the experimental glasses suggest, that the evaporation rates are slower than B_2O_3 diffusion rates, and therefore the rate limiting process. Overall, the rate of B evaporation in air is approximately an order of magnitude higher compared to reducing conditions at FMQ-4.

1. Introduction

Boron is an integral component in many industrial glasses, because of its enhancing effect on the thermal, mechanical, and optical glass properties. Borosilicate

glasses find wide applications in cook- and labware, fiberglass, displays, and optical components because of their high thermal shock resistance and chemical inertness ([1]). The usage of B benefits the glass making process in several ways, for example by lowering the melting/liquidus temperature and viscosity of the melt or allowing the dissolution of refractory oxides (for a review refer to [1]; [2]; [3]). The reduction of the liquidus temperature by the addition of B has also proven useful in petrological experimental studies and enabled the synthesis of large quantities of volatile bearing glasses at atmospheric pressures (e.g., [4], [5]).

Boron is considered a network former in both silicate and aluminosilicate glasses ([6], [7], [8], [9], [10]). Additionally, B is classified as a volatile species in both the glass-manufacturing industry and in cosmochemistry (classified as volatile lithophile element, with a 50% condensation temperature (T_{50}) from a solar nebula gas at 10^{-4} bar, at 635 °C, [11]; 467 °C, [12]). The most abundant B species in glasses and melts are three-fold and four-fold coordinated by O^{2-}. In borosilicate glasses, speciation of B changes mostly as a function of the composition (e.g., SiO_2 and alkali element content, [1], [13], [14], [15] and references therein) and it controls the molecular structure of the glass/melt and the interconnectivity of B_2O_3 and SiO_2 networks. The arrangement of this network will in turn govern the extent of B degassing from the melt. But fO_2 is known to affect the speciation of elements in melts, which raises the question to what degree B is lost to a gas phase from a borosilicate melt at high temperatures, (such as during glass synthesis) and what is the effect of fO_2 on the evaporation process.

Here, we present a novel dataset on the evaporation behavior of B from B-, Ca-, and Mg-bearing aluminosilicate melt at 1250 and 1350 °C, over 60, 120, 240, and 1020 minutes, in air and at logfO_2 relative to the fayalite-magnetite-quartz buffer (FMQ), of ΔFMQ = +1.5 (hereafter written as FMQ+1.5), FMQ, FMQ-2, FMQ-4, and FMQ-6.

2. Materials and Methods

2.1 Starting Material

Evaporation experiments were performed using a CaO-MgO-SiO_2-Al_2O_3-B_2O_3 glass as the starting material. The composition was at the anorthite ($CaAl_2Si_2O_8$) – diopside ($CaMg_2Si_2O_6$) eutectic at $An_{36}Di_{64}$ (in mol%), to which ~ 10wt.% B_2O_3 were added. The starting material was prepared using analytical grade oxides (MgO, SiO_2, Al_2O_3; Sigma-Aldrich, GmbH, Germany), carbonate ($CaCO_3$ Alfa; Aesar GmbH, Germany) while B was added as boric acid (H_3BO_3; ABCR-GmbH, Germany). To release any adsorbed water or hydroxides, MgO was fired at 1000 °C for more than 12 h and subsequently stored at 110 °C in a drying cabinet. The starting material mixture was then fired at 1000 °C for 3 h to decarbonate the $CaCO_3$ and to convert the H_3BO_3 to B_2O_3 ([16]). The resulting mixture was reground under ethanol, vitrified at 1200 °C in a Pt-Au crucible for 30 minutes and quenched in cold water. For the vitrification we used a Linn HighTherm VMK1800 (Linn GmbH, Germany) box furnace. A detailed description of the starting material glass synthesis is given in [4].

The resulting glass (PPG14) was crushed into shards in an agate mortar and was investigated texturally using a JEOL scanning electron microscope (SEM) ([4]). The

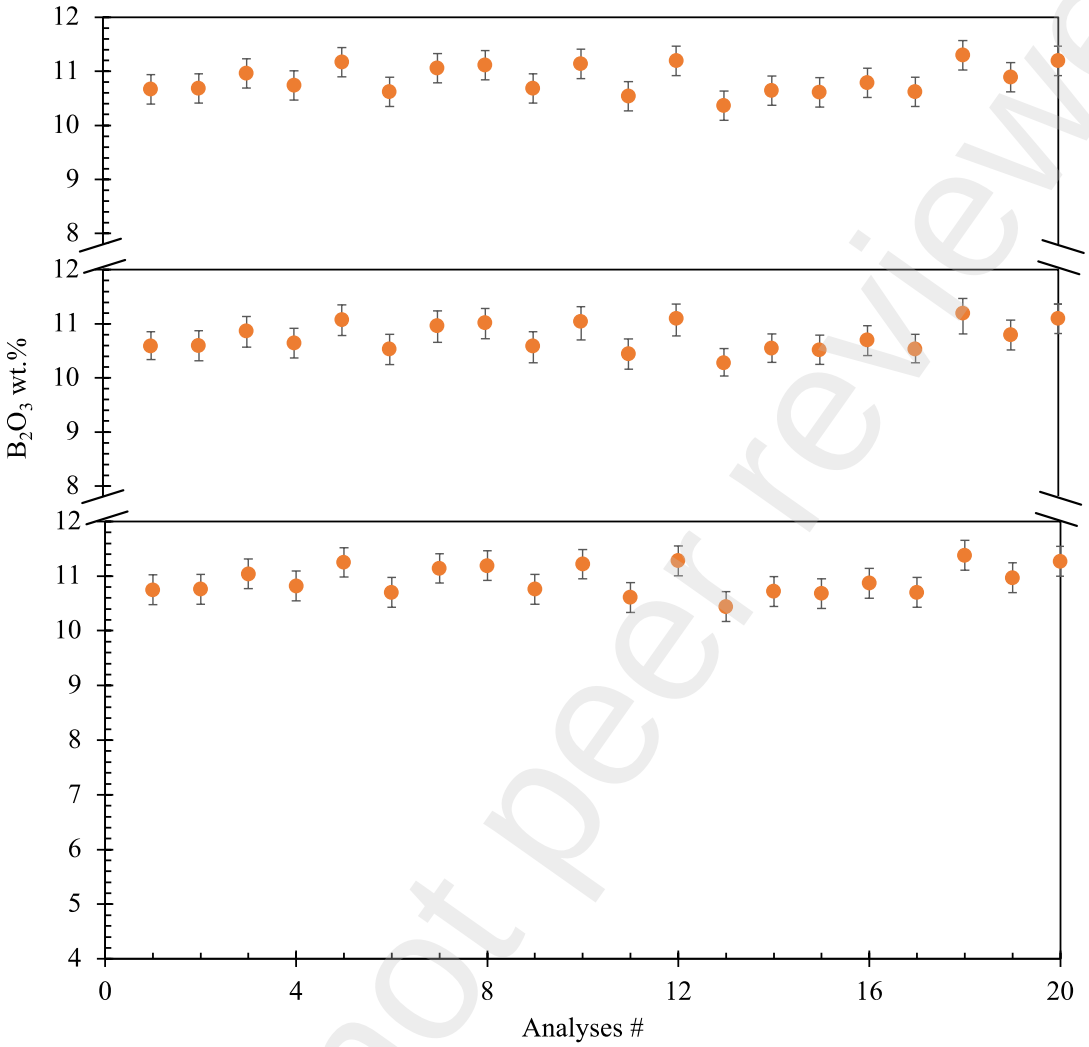

chemical composition and homogeneity of the glass was confirmed by electron microprobe analysis (EMPA) profile analyses across random shards (Fig. 1).

Fig. 1 Homogeneity of the starting material verified by profile analyses of different shards. Three profile analyses were made, from center to rim, in three random glass shards. All these profiles show no diffusional zonation (analyses # 20).

A sum of 60 analyses (n=60, 20 in each shard) testify to the homogeneity of the starting glass (Table A.1). We determined an initial B_2O_3 concentration of 10.78 ± 0.27 wt.% (SD). The composition of the starting mixtures and the median composition of the synthesized glass are given in Table 1.

Table 1 Starting mixture compositions and EPMA analyses of synthesized glass

Analyses (wt.%)	An_{36}-Di_{64}	Normalized Start. Mix.	Synth. Glass (PPG14)	
			Median	SD
SiO_2	50.33	35.58	46.23	0.17
Al_2O_3	15.37	10.87	13.83	0.06
MgO	10.80	7.64	9.57	0.04
CaO	23.49	29.64	20.99	0.07
B_2O_3	-	16.27	10.78	0.27
Total	100.00	100.00	101.40	0.36

Table 1 the first two columns show the calculated composition of the anorthite-diopside eutectic and the normalized starting mixture respectively. The last column shows the EPMA data of the synthesized glass. Errors reported are SD.

3. Experimental techniques

Glass shards with diameters of ~2 mm were singled out for the experiments. The shards were hooked on Pt-wire loops with a diameter of 0.1 mm. For each experimental condition, the sample was suspended on a Pt-chandelier on an alumina rod. The experiments were conducted in a vertical gas-mixing tube furnace (Gero GmbH, Germany) and oxygen fugacity was controlled by mixing CO and CO_2 gases using a Tylan mass flow controller. Temperatures within the furnace were monitored and controlled by a $Pt_{70}Rh_{30}$–$Pt_{94}Rh_6$ (type B) thermocouple connected to a Eurotherm 2416 (Schneider Electric Systems, Germany) controller. The furnace was pre-heated to the given temperature at least 30 min before the experiments to ensure that it was thermally equilibrated and that temperature variations within the furnace's hot zone were negligible. Gases were introduced at the top of the tube furnace with an outflow at the lower end of the furnace. Oxygen fugacity varied between air and -13.3 $\log f O_2$ units relative to the Fayalite-Magnetite-Quartz (FMQ) buffer system (Table 2). The samples were initially placed in the cold zone of the furnace to allow the CO-CO_2 gas

mixture to equilibrate for ~ 2 minutes. The samples were then lowered into the hot zone of the furnace where they degassed for different time durations (60-1020 minutes, Table 2). The runtime of each experiment was considered from the time of introducing the sample into the hot zone of the furnace. During the experiments, temperature was monitored and controlled by an external Type B thermocouple connected to a Eurotherm controller. During the run, temperature variations were less than ±1 °C. Experiments were stopped by turning off the gas flow ~40 seconds before opening the furnace lid and quenching the sample in a cold-water bath. Each sample was then used for characterization by SEM, EMPA, and LA-ICP-MS (Laser-Ablation Inductively Coupled Mass Spectrometry).

Two types of experimental series have been conducted at 1245 °C and 1361 °C namely "fO_2 series" and "t series". In the former, fO_2 varies between oxidizing and reducing conditions (air to FMQ-6), while the run duration remains constant (60 min). In the latter, it is fO_2 that remains constant, while run durations vary from 60 to 1020 minutes. This approach allows us to examine the effects of both fO_2 and time on the evaporation of B. Importantly, these experiments are run in an open system with constant flow of CO and CO_2 gas, allowing efficient evaporative loss of B from the melt.

4. Analytical Methods

For each experimental run one sample was characterized in cross-section with a JEOL 6510 LA scanning electron microscopy (SEM), and the chemical homogeneity was investigated with a 5-spectrometer JEOL JXA 8530F electron microprobe analyzer (EMPA) and laser ablation inductively coupled plasma mass spectrometry (LA-ICP-MS) at the Institut für Mineralogie, Westfälische Wilhelms-Universität Münster. The

SEM back-scattered electron images were taken at an acceleration voltage of 20 kV and a working distance of 10 mm.

The EMPA measurements were made at an acceleration voltage of 15 kV, 60 nA beam current, and a 10 µm beam size. Boron was measured for 120 s on the peak and 60 s on the background. The Astimex BN has been used a standard for the EMPA measurements. The other elements (Ca, Mg, Si, Al) were measured for 20 s on the peak and 10 s on the background.

For the LA-ICP-MS measurements, the polished samples were ablated in a dual-volume Helex cell (He gas flux of 1 L/min in the large cell and 0.33 L/min in the small cell). We used a Photon Machines Analyte G2 193 nm ArF excimer laser system at a pulse rate of 10 Hz and a spot size of 50 µm. The ablated material was analyzed in a Thermo Fisher Element II, measuring 20 s background and 40 s sample counting time. The isotopes measured were ^{29}Si, and ^{11}B, where ^{29}Si was used as the internal standard. The primary standard analyzed was NIST610 (350 ± 7 ppm B, [17]), and NIST612 (34.6 ± 0.78 ppm B, [18]).

5. Results

5.1 Boron evaporation and concentrations of residual glasses

All our experimental run conditions and results are given in Table 2. Boron data were obtained using EMPA and LA-ICP-MS profiles (step size and profile lengths in Table A.2) on the cross-sectioned samples of all experiments. The relative loss of B_2O_3 in the final glass compared to the initial content in the starting material is reported as X_t/X_0 and $\ln(X_t/X_0)$ in Table 2.

Before assessing the role of fO_2, T and run time in our experiments we need to consider whether the changing B contents of the glasses were controlled by the

evaporation reaction, or diffusion from the melt interior to the evaporation surface. To that end we measured diffusion profiles in both the "fO_2 series" and "t series" (Fig. 2) experiments. At all experimental conditions, the investigated samples showed no indication of zoning and concentrations are constant within error for all the samples. Therefore, these profiles rule out any effect of diffusion on the B contents of the glasses, which implies that the evaporation rate is lower than the diffusion rate of B in the glass. Hence, diffusion is not the rate limiting factor of B evaporation at high temperatures (1245 – 1361 °C).

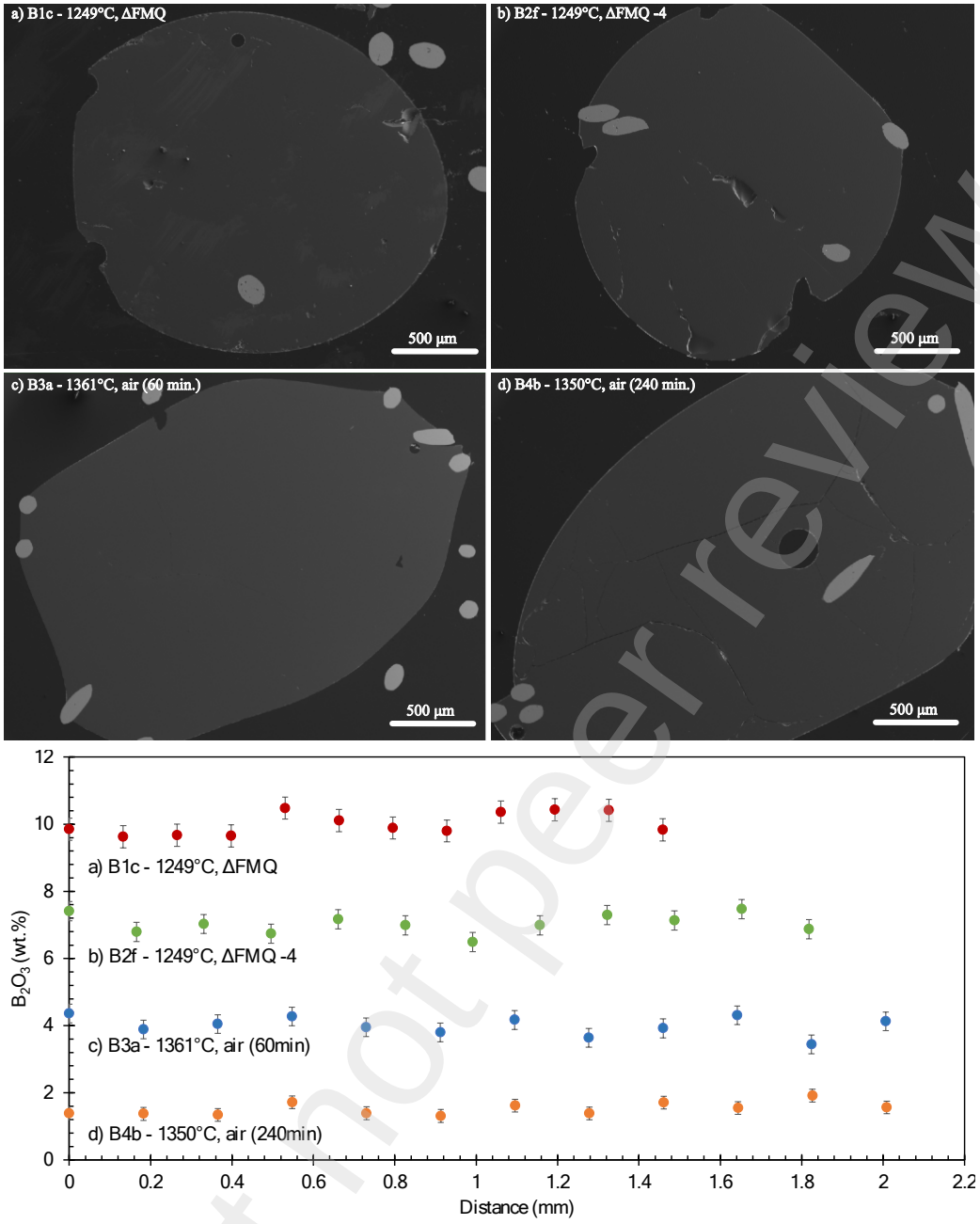

157

158 **Fig. 2** Scanning electron (SE) and backscattered electron images (BSE) (a-d), and profile
159 analyses of the "fO_2 series" and "t series" experiments. a) and b) show SE images of glass
160 shards from the "fO_2" series experiments at 1249 °C in FMQ and FMQ-4 respectively. Time
161 duration of both the experimental runs was 60 minutes. c) BSE image and d) SE image, of runs
162 from the "t series" experiments in air at 1350 °C and 1361 °C respectively. Time duration of
163 these experimental runs varied from 60 to 1020 minutes (here the 60 and 240 min runs). e)
164 EPMA and LA-ICP-MS measurement profiles from the center of the experimental beads. The
165 profiles show no diffusional zonation from the center to the rim (analyses # 14).

Table 2 Experimental runs and conditions. Boron concentrations in wt%. Errors reported are SD.

Exp. Series	Glass #	Exp. #	T(°C)	fO_2 (ΔFMQ)	log(fO_2)	t (min)	B_2O_3	Error	(Xt/X_0)	Error	ln(Xt/X_0)	Error (+)	Error (-)
fO_2 series	B1	B1a	1245	6.62	-0.68	60	8.74	0.76	0.81	0.07	-0.21	0.086	0.095
	B1	B1b	1249	1.5	-6.3	60	10.32	0.78	0.96	0.08	-0.04	0.076	0.083
	B1	B1c	1249	0	-7.8	60	10.33	0.78	0.96	0.08	-0.04	0.076	0.083
	B1	B1d	1249	-2	-9.8	60	10.65	0.79	0.99	0.08	-0.01	0.075	0.081
	B1	B1e	1249	-4	-11.8	60	10.56	0.78	0.98	0.08	-0.02	0.075	0.082
	B1	B1f	1249	-6	-13.8	60	10.95	0.79	1.02	0.08	0.02	0.073	0.079
fO_2 series	B3	B3a	1361	5.62	-0.68	60	3.95	0.69	0.37	0.06	-1.00	0.163	0.194
	B3	B3b	1361	1.5	-5.3	60	8.24	0.75	0.76	0.07	-0.27	0.090	0.099
	B3	B3c	1361	0	-6.8	60	8.84	0.76	0.82	0.07	-0.20	0.086	0.094
	B3	B3d	1361	-2	-8.8	60	9.03	0.75	0.84	0.07	-0.18	0.084	0.091
	B3	B3e	1361	-4	-10.8	60	9.19	0.76	0.85	0.07	-0.16	0.083	0.090
	B3	B3f	1361	-6	-12.8	60	10.01	0.77	0.93	0.08	-0.07	0.078	0.084
t series	B1	B1a	1245	6.62	-0.68	60	8.74	0.76	0.81	0.07	-0.21	0.086	0.095
	B2	B2a	1245	6.62	-0.68	120	6.78	0.73	0.63	0.07	-0.46	0.105	0.118
	B2	B2b	1245	6.62	-0.68	240	5.22	0.71	0.48	0.07	-0.72	0.130	0.149
	B2	B2c	1245	6.62	-0.68	1020	0.37	0.02	0.03	0.00	-3.37	0.052	0.055
t series	B1	B1e	1249	-4	-11.8	60	10.56	0.78	0.98	0.08	-0.02	0.075	0.082
	B2	B2d	1249	-4	-11.8	120	9.76	0.77	0.91	0.08	-0.10	0.080	0.087
	B2	B2e	1249	-4	-11.8	240	9.40	0.77	0.87	0.07	-0.14	0.082	0.089
	B2	B2f	1249	-4	-11.8	1020	7.03	0.73	0.65	0.07	-0.43	0.102	0.113
t series	B3	B3a	1361	5.62	-0.68	60	3.95	0.69	0.37	0.06	-1.00	0.163	0.194
	B4	B4a	1350	5.62	-0.68	120	2.61	0.11	0.24	0.01	-1.42	0.048	0.050
	B4	B4b	1350	5.62	-0.68	240	1.22	0.06	0.11	0.01	-2.18	0.050	0.053
	B4	B4c	1350	5.62	-0.68	1020	0.006	0.000	0.001	0.00	-7.43	0.056	0.060
t series	B3	B3e	1361	-4	-10.8	60	9.19	0.76	0.85	0.07	-0.16	0.083	0.090
	B4	B4d	1361	-4	-10.8	120	8.37	0.76	0.78	0.07	-0.25	0.090	0.099
	B4	B4e	1361	-4	-10.8	240	7.78	0.75	0.72	0.07	-0.33	0.095	0.105
	B4	B4f	1361	-4	-10.8	1020	3.30	0.68	0.31	0.06	-1.18	0.190	0.235

The experimental results in the "fO_2 series" runs are presented in Figure 3. These experiments show that B degassing increases with increasing fO_2 (from FMQ-6 to air) and with increasing temperatures (from 1249 °C to 1361 °C).

At 1249 °C and from highly reducing to slightly oxidizing conditions (FMQ-6 to ~ FMQ+1.5) B is degassed up to ~ 0.6 wt.% (0.02 to 0.04% is the relative loss). At the same temperature and oxidizing conditions (in air), B is degassing to about ~ 2 wt.% (20% relative loss) bringing the final B-concentration of the sample down to ~ 8.7 wt.%.

At 1361 °C and from FMQ-6 to ~ FMQ+1.5, around 2 wt.% of the initial B content is lost (~ 20% relative loss) as the samples show a content of ~ 8.2 wt.%. At the same temperature in air, the B-loss has increased by almost an order of magnitude, resulting in a loss of around 6 wt.%, which attributes for the ~ 60% of the initial B content leaving the final glass with ~ 4 wt.% B.

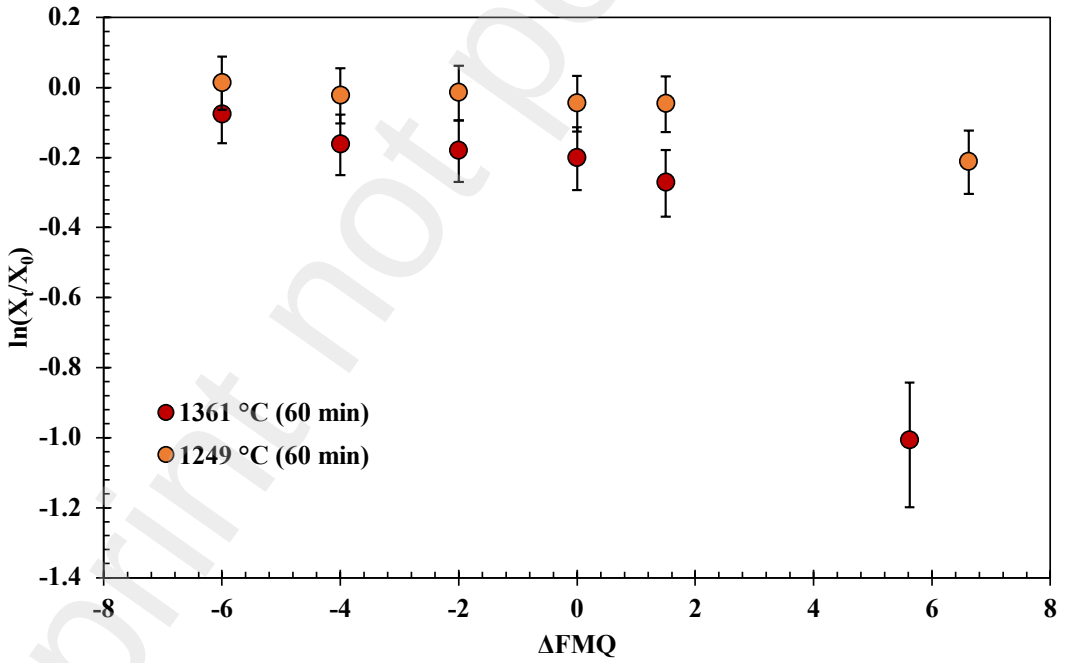

Fig. 3 Experimental results of the "fO_2 series" runs. The natural logarithm of the ratio of the final (X_t) versus the initial (X_o) B_2O_3 concentration of the glasses is plotted against the fO_2 (relative to the FMQ buffer) of the runs.

The experimental results from the "t series" runs (Fig. 4) show that B degassing increases with longer run times (60 to 1020 min), higher temperatures (1245 °C to 1361 °C), and with increasing fO_2 (from air to FMQ-4). The extent of degassing varies between the different run durations, temperatures and fO_2 conditions.

At 1249 °C and reducing conditions (FMQ-4), and run durations between 60 and 240 minutes, ~ 1wt.% B is lost due to degassing or ~ 9% compared to its initial concentration. In the 1020 minutes experiment (same T and fO_2 conditions) the amount of degassed B has increased to an absolute value of ~ 3wt.% or ~ 25% relative. At the same temperature (1245 °C) but at oxidizing conditions (i.e., air) B degasses more strongly with an absolute loss of ~ 2 wt.% (20% relative) after 60 min, ~ 3wt.% (~ 30% relative) after 120 min, and ~ 5wt.% (50% relative) after 240 min. The 1020 min run shows an almost complete loss of the initial B content i.e., from ~ 10 wt.% down to 0.37 wt.% (~ 96% relative loss).

At 1361 °C and reducing conditions (FMQ-4), and run durations between 60- and 240 minutes, the B content of the degassed glass has decreased by ~ 2.2 wt.%, or 22% relative. At the same conditions in the 1020 minutes experiment, the sample has lost more than half of its initial B concentration, ~ 6.7 wt.% (~ 70% relative). At 1350 °C in air B, degassing is extensive resulting in a loss of ~ 6 wt.% (60% relative) in the 60 minutes run, ~ 7.5 wt.% in the 120 minutes run, and 8.8 wt.% in the 240 minutes run. In the 1020 minutes run B is almost completely lost from the glass, ~ 10.77 (~ 99.9% relative loss) leaving but only 0.006 wt.% B in the final glass.

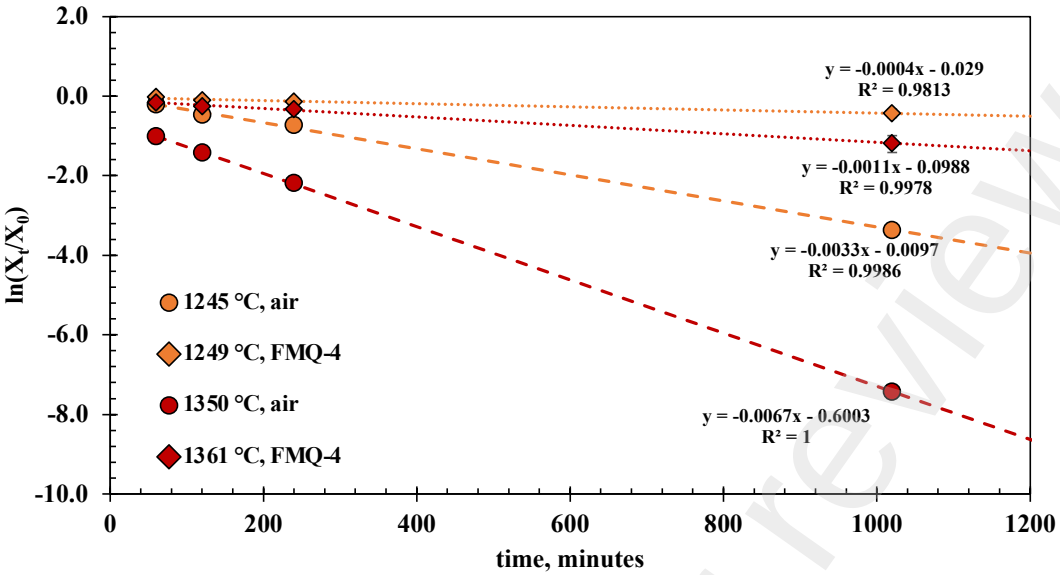

Fig. 4 The results of the "t series" runs. The natural logarithm of the B_2O_3 concentration in the glasses is plotted against different run durations. The error bars are only plotted when larger than the symbols.

6. Discussion

6.1 Evaporation rate constant

To assess the effect of temperature and fO_2 on the evaporation of B we calculated the evaporation rate constants k_i from the time series experiments using the equation of [19] as used by [20]:

$$ln\left(\frac{X_t}{X_0}\right) = -3k_i t/r \quad (1)$$

For these calculations we treat each sample as a liquid sphere with an average radius of 0.01 cm and assume that the activity coefficient of B_2O_3 in each experiment remains constant. X_t and X_0 are the concentrations in the final and starting glass respectively, k_i is the evaporation rate constant, t is the time of the run and r the radius of the liquid sphere. Table 3 shows the evaporation rate constants of B_2O_3 from the "t series" runs, which were calculated by linear regression from the slopes ($-3k_it/r$) of the trendlines in

Figure 4. The calculated evaporation rate constants demonstrate that oxygen fugacity, ranging from air ($\log fO_2 = -0.68$) to FMQ-4, plays a key role in B evaporation. The difference in evaporation rate constant of an order of magnitude between very oxidizing (in air) and very reducing (FMQ-4) conditions requires a mechanistic explanation. In the next section we discuss how the speciation of B in the gas phase and the respective evaporation reactions differ at the two experimentally investigated redox conditions.

Table 3 Calculated evaporation rate constants, k_i, for B in the "t series" experiments

Glass #	Exp. #	T(°C)	ΔFMQ	k_i (cm/min)	r (cm)	Slope
B1, B2	B1a, B2a, b, c	1245	in air	1.09×10^{-5}	0.01	-3.28×10^{-3}
B1, B2	B1e, B2d, e, f	1249	-4	1.31×10^{-6}	0.01	-3.94×10^{-4}
B3, B4	B3a*, B4a, b, c	1350, 1361*	in air	2.23×10^{-5}	0.01	-6.69×10^{-3}
B3, B4	B3e, B4d, e, f	1361	-4	3.54×10^{-6}	0.01	-1.06×10^{-3}

6.2 Evaporation reactions

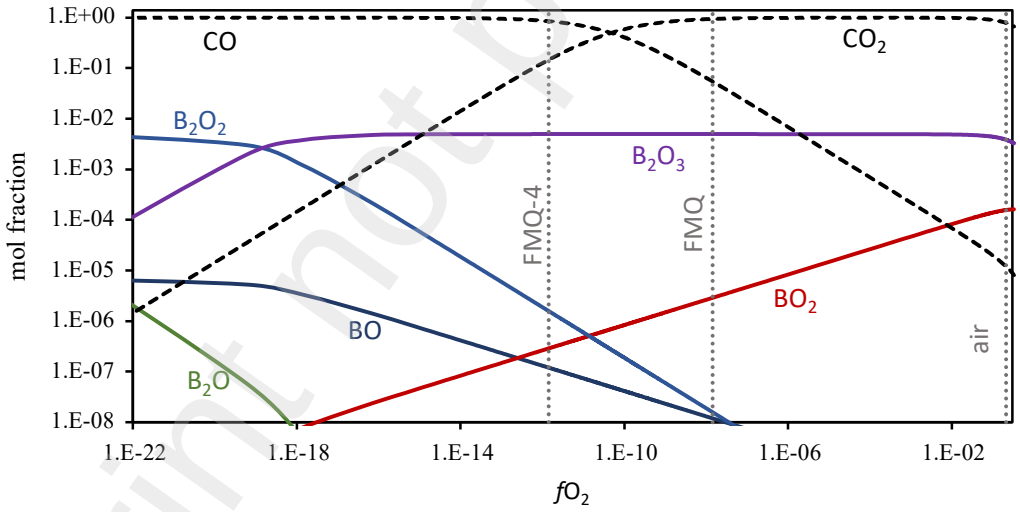

Fig. 5 Boron gas-phase speciation at 1250 °C as a function of fO_2. Gibbs free energy minimization calculation results are shown as mol fractions. The dotted vertical lines show the fO_2 of air, FMQ, and FMQ-4. Stippled lines show the mol fractions of CO and CO_2, the gases that were used to control fO_2 in the evaporation experiments. The relative amount of the different B gas species are shown on solid lines. In the presented range of mol fractions and fO_2 the stable gas species are B_2O_3, BO_2, B_2O_2, BO, and B_2O. The full calculation results are included in Table A.3.

Boron shows a redox-sensitive behavior as its loss is more pronounced at highly oxidizing conditions (Figs. 3, 4). The evaporation mechanism and rate depend on the stoichiometry of the evaporation reactions which in turn are dictated by the speciation and valence state of the element in the melt and in the gas phase (e.g., [21]). To constrain the B gas-phase speciation we conducted Gibbs free energy minimization calculations using the software package HSC Chemistry 9 ([22]). The thermodynamic database of HSC is largely based on NIST-JANAF data ([23]). We conducted calculations at 1250 and 1350 °C, including the gas species CO_2, CO, O_2, O_3, B, B_2, BC, BC_2, B_2C, BCO, BO, BO_2, B_2O, B_2O_2, and B_2O_3. The oxygen fugacity was varied by step-wise adding O_2 to CO, and ranges from $\log fO_2 = -26$ to $\log fO_2 = -0.5$. The detailed results of the calculations are provided in Table A.4. The dominant B gas-species at $\log fO_2 > -18$ conditions relevant for all our experiments, is B_2O_3. At even more reducing conditions the primary gas species becomes B_2O_2, with minor abundances of BO, B_2O, BC_2, and B_2C. At increasingly oxidized conditions BO_2 becomes an important minor gas species, and it is most relevant at highly oxidizing conditions, such as in our experiment in air. If we then assume that B occurs only as B_2O_3 in the melt phase, we can write the following two evaporation reactions for the two most abundant gas species B_2O_3 and BO_2:

a) $B_2O_3\ (\ell) = B_2O_3\ (g)$

b) $B_2O_3(\ell) + ½\ O_2\ (g) = 2\ BO_2\ (g)$

In reaction (a) B is in a trivalent state (B^{3+}) in both the melt and the gas phase. This evaporation reaction is independent of the fO_2 and predominates in all our experiments. The independence of reaction (a) from fO_2 is evident in Figure 3, where the data show almost flat trends as fO_2 varies from FMQ-6 to FMQ+1.5. However, a minor increase in volatility of B with increasing fO_2 can be observed in the data. We attribute this

increase, as well as the high rate of B evaporation in air (Figure 3) to the increasing stability of BO_2 at high fO_2 towards air. Reaction (b) thus describes the fO_2 dependent evaporation of B in the oxidized tetravalent (B^{4+}) state. BO_2 is observed in high temperature B combustion experiments, but it's not stable as a solid ([24]).

In conclusion, at relatively reducing conditions (FMQ-4 to ~ FMQ+1) one species of B predominates (B_2O_3). On the other hand, at highly oxidizing conditions (above FMQ+1.5 to air) two species of B are important in the gas phase i.e., B_2O_3 and BO_2, indicating the presence of two different valence states (B^{3+} and B^{+4}).

6.3 Implications for evaporative B loss from large industrial volumes of melt

By conducting time series evaporation experiments we derived the kinetic evaporation rates of B from aluminoborosilicate melts at 1250 and 1350 °C for two different redox states, in FMQ-4 and in air (Table 3). Our experiments further demonstrate that the evaporation is not rate limited by B diffusion in the melt. This observation provides a lower limit on B diffusion estimates.

To assess the extent to which B is lost at industrial scale we use the determined evaporation rate constants and apply them to a simple model (Fig. 6). In this model we assume spherical samples with radii ranging from 0.01 cm to 1000 cm. We use the evaporation rate constants (Table 3) from the "1350 °C – in air" and "1350 °C – FMQ-4" experiments, i.e., 2.23×10^{-5} and 3.54×10^{-6} (cm/min) and different sample radii, in equation (1), to calculate degassing times (Table 4). In this way, we determine the time needed for each sample, depending on its radius, to lose 5% and 50% of its initial B_2O_3 content by evaporation of $B_2O_{3(g)}$ and $BO_{2(g)}$ (Fig. 6).

Table 4 Evaporation rates of B_2O_3 from samples with different radii at different fO_2 conditions

			1350 °C – air		1350 °C –FMQ-4	
r (cm)	**log (r)**	**loss %**	**days**	**log (days)**	**days**	**log (days)**
0.01	-2	5	0.01	-2.27	0.03	-1.47
		50	0.07	-1.14	0.45	-0.34
0.1	-1	5	0.05	-1.27	0.34	-0.47
		50	0.73	-0.14	4.54	0.66
1	0	5	0.54	-0.27	3.4	0.53
		50	7.3	0.86	45	1.66
10	1	5	5.4	0.73	33	1.53
		50	73	1.86	453	2.66
100	2	5	54	1.73	335	2.53
		50	729	2.86	4535	3.66
1000	3	5	539	2.73	3356	3.53
		50	7293	3.86	45357	4.66

Even though evaporative B loss is significant at the small sample scale of our experiments, the determined rate constants are very low. In small volume samples like in the present study (i.e., r = 0.1 cm), exposure at 1350 °C and oxidizing conditions (in air), will result in a loss of 5% of B_2O_3 in only 8 minutes. At the same conditions, the threshold of the 50% loss will be reached in 105 minutes. At reducing conditions (FMQ-4), for the same sample size (r = 0.01 cm) and temperature, the time needed to lose 5% and 50% of the initial B content is 48 and 653 minutes. What we observe here is a 6-fold increase in the exposure times between oxidizing and reducing fO_2 conditions, to reach the same amount of B loss. At industrial volumes of melt on the order of cubic meters (in our model represented by the 100 cm and 1000 cm sample radii) extensive exposure at 1350 °C and oxidizing conditions of ~ 2 to ~ 20 years (Figure 6; Table 4; Table A.4) would be necessary to result in B loss of 50% of the initial content). Importantly, our experiments are conducted in an open system where the evaporated gas phase is efficiently transported away from the melt. In a closed large

volume furnace typically used in industrial processes this condition is not met. Our calculated rates of B loss are therefore upper limit estimates.

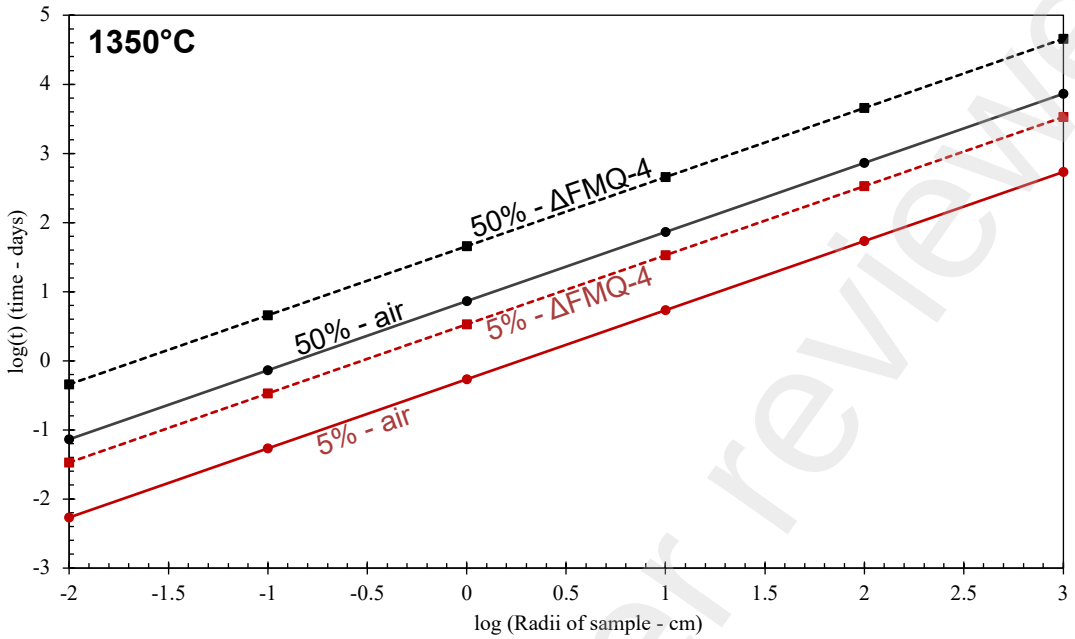

Fig. 6 Evaporation rate models of aluminoborosilicate glasses with different radii at 1350 °C for oxidizing and reducing fO_2 conditions (in air and FMQ-4 respectively). Continuous lines represent the evaporation rate models for the experimental runs at oxidizing conditions (air). Dashed lines represent the evaporation rate models for the experimental runs at reducing conditions (FMQ-4). Red lines show the time it will take depending on the sample radii, for the melt to lose due to degassing 5% of its initial B_2O_3 content, while black lines represent the 50% loss of the initial B_2O_3 content of the sample.

In summary, our study indicates that under oxidizing conditions B_2O_3 degassing will increase by an order of magnitude. During the synthesis of aluminoborosilcate glasses, these losses might have important implications for the melt composition and hence, the structure and the properties of the final glass. In large volume samples used in industrial glass making, these losses are not so extensive, but they might generate smaller degassing surfaces which in turn might create local deviations from the intended glass composition and consequently its expected properties.

7. Conclusions

- At high temperatures of 1350 °C and very oxidizing conditions in air, the alkaline-bearing aluminoborosilicate melt entirely loses its B content by evaporation within 1020 minutes.
- Evaporation rate constants along with the sample size can be used to determine the rate and amount of B loss
- Small scale samples are more prone to evaporation losses
- Large scale samples may generate local degassing surfaces that can affect locally the composition and structure, and by that the properties of the final glass.

CRediT author contribution statement

Stamatis Flemetakis: Conceptualization, Methodology, Formal analysis, Investigation, Writing - Original Draft, Visualization **Christian Renngli:** Conceptualization, Methodology, Formal analysis, Investigation, Software, Writing - Review & Editing, Funding acquisition **Paul Pangritz:** Formal analysis, Investigation **Jasper Berndt:** Investigation, Resources, Writing - Review & Editing **Stephan Klemme:** Supervision, Funding acquisition

Acknowledgements

We acknowledge funding by the Deutsche Forschungsgemeinschaaft (DFG, German Research Foundation - SFB-TRR 170). CR is funded by the DFG – project 442083018. Our thanks go M. Feldhaus, J. Kemmann, M. Trogisch, B. Schmitte, and P. Weitkamp for excellent sample preparation, and maintenance and repairs of the

experimental and analytical facilities at the Institut für Mineralogie at WWU Münster.

This is SFB-TRR 170 publication No…

References

[1] M. Hubert, A.J. Faber, On the structural role of boron in borosilicate glasses, Physics and Chemistry of Glasses. 55 (2014) 23.

[2] R.A. Smith, Boron in Glass and Glass Making, Journal of Non-Crystalline Solids. 84 (1986) 421–432.

[3] J.E. Shelby, Introduction to Glass Science and Technology, The Royal Society of Chemistry, 2015.

[4] P. Pangritz, C.J. Renggli, J. Berndt, A. Rohrbach, S. Klemme, Synthesis of Large Amounts of Volatile Element-Bearing Silicate Glasses Using a Two-Stage Melting Process, ACS Earth Space Chem. 6 (2022) 1108–1114. https://doi.org/10.1021/acsearthspacechem.2c00020.

[5] C.J. Renggli, J.L. Hellmann, C. Burkhardt, S. Klemme, J. Berndt, P. Pangritz, T. Kleine, Tellurium isotope fractionation during evaporation from silicate melts, Geochimica et Cosmochimica Acta. 339 (2022) 35–45. https://doi.org/10.1016/j.gca.2022.10.032.

[6] Uhlmann D. R. & Kreidl, N. J. (1983) Glass Forming Systems. Glass Science and Technology. Edited by Academic Press, New York, USA, Vol. 1, 465.

[7] A.C. Hannon, R.N. Sinclair, J.A. Blackman, A.C. Wright, F.L. Galeener, Phonon spectra of vitreous B2O3, Journal of Non-Crystalline Solids. 106 (1988) 116–119. https://doi.org/10.1016/0022-3093(88)90242-6.

[8] A.C. Hannon, A.C. Wright, J.A. Blackman, R.N. Sinclair, The vibrational modes of vitreous B2O3: inelastic neutron scattering and modelling studies, Journal of Non-Crystalline Solids. 182 (1995) 78–89. https://doi.org/10.1016/0022-3093(95)00577-3.

[9] M. Micoulaut, R. Kerner, D.M. dos Santos-Loff, Statistical modelling of structural and thermodynamical properties of vitreous B2O3, J. Phys.: Condens. Matter. 7 (1995) 8035. https://doi.org/10.1088/0953-8984/7/42/002.

[10] B.L. Shivachev, I.P. Mincov, E.P. Kashchieva, Y.B. Dimitriev, R. Smith, T. Troev, Positron lifetime spectroscopy of vitreous B2O3, Journal of Non-Crystalline Solids. 345–346 (2004) 108–111. https://doi.org/10.1016/j.jnoncrysol.2004.08.004.

[11] K. Lodders, Solar System Abundances and Condensation Temperatures of the Elements, Astrophysical Journal 591 (2003) 1220. https://doi.org/10.1086/375492.

[12] B.J. Wood, D.J. Smythe, T. Harrison, The condensation temperatures of the elements: A reappraisal, American Mineralogist. 104 (2019) 844–856. https://doi.org/10.2138/am-2019-6852CCBY.

[13] M. Lenoir, A. Grandjean, Y. Linard, B. Cochain, D.R. Neuville, The influence of Si,B substitution and of the nature of network-modifying cations on the

properties and structure of borosilicate glasses and melts, Chemical Geology. 256 (2008) 316–325. https://doi.org/10.1016/j.chemgeo.2008.07.002.

[14] J.A.C. van Limpt, Modeling of evaporation processes in glass melting furnaces, Phd Thesis 2 (Research NOT TU/e / Graduation TU/e), Technische Universiteit Eindhoven, 2007. https://doi.org/10.6100/IR630685.

[15] H. van Limpt, R. Beerkens, S. Cook, R. O'Connor, J. Simon, Modelling the evaporation of boron species. Part 1. Alkali-free borosilicate glass melts, Glass Technology. 52 (2011) 11.

[16] C. Huber, S.S. Jahromy, F. Birkelbach, J. Weber, C. Jordan, M. Schreiner, M. Harasek, F. Winter, The multistep decomposition of boric acid, Energy Science & Engineering. 8 (2020) 1650–1666. https://onlinelibrary.wiley.com/doi/abs/10.1002/ese3.622 (accessed November 24, 2022).

[17] K.P. Jochum, U. Nohl, K. Herwig, E. Lammel, B. Stoll, A.W. Hofmann, GeoReM: A New Geochemical Database for Reference Materials and Isotopic Standards, Geostandards and Geoanalytical Research. 29 (2005) 333–338. https://doi.org/10.1111/j.1751-908X.2005.tb00904.x.

[18] Y. Kusano, S. Umino, R. Shinjo, A. Ikei, Y. Adachi, S. Miyashita, S. Arai, Contribution of slab-derived fluid and sedimentary melt in the incipient arc magmas with development of the paleo-arc in the Oman Ophiolite, Chemical Geology. 449 (2017) 206–225. https://doi.org/10.1016/j.chemgeo.2016.12.012.

[19] A. Tsuchiyama, H. Nagahara, I. Kushiro, Volatilization of sodium from silicate melt spheres and its application to the formation of chondrules, Geochimica et Cosmochimica Acta. 45 (1981) 1357–1367.

[20] B.A. Cohen, R.H. Hewins, C.M.O. Alexander, The formation of chondrules by open-system melting of nebular condensates 1 1Associate editor: C. Koeberl, Geochimica et Cosmochimica Acta. 68 (2004) 1661–1675. https://doi.org/10.1016/j.gca.2003.09.009.

[21] P.A. Sossi, S. Klemme, H.S.C. O'Neill, J. Berndt, F. Moynier, Evaporation of moderately volatile elements from silicate melts: experiments and theory, Geochimica et Cosmochimica Acta. 260 (2019) 204–231.

[22] HSC Chemistry 9 [Computer software] (2018) Metso:Outotec. http://www.mogroup.com/portfolio-chemistry/

[23] Chase M.W., (1998) NIST-JANAF Thermochemical Tables. Physical and Chemical Reference Data.

[24] Dreizin E.L., Keil D.G., Felder W., Vicenzi E.P. (1999) Phase changes in boron ignition and combustion. Combustion and Flame 119, 272-290